

The Study of Low Temperature Austenite Decomposition in a Fe-C-Mn-Si Steel Using the
Neutron Bragg Edge Transmission Technique

J. Huang¹, S.C. Vogel², W.J. Poole¹, M. Militzer¹, and P. Jacques³

1. The Centre for Metallurgical Process Engineering, The University of British Columbia, Vancouver, B.C., V6T 1Z4, Canada
2. The Los Alamos Neutron Scattering Centre, Los Alamos National Laboratory, Los Alamos, NM, 87545, USA
3. Département des Sciences and Matériaux ed des Procédés, Université Catholique de Louvain, B-1348 Louvain-la-Neuve, Belgium.

Introduction

1.1 Low temperature austenite decomposition and TRIP steels

There is currently significant interest in developing new steels with improved combinations of strength and ductility/formability, particularly for applications in the transportation sector where weight reduction is the most effective way to decrease the environmental impact of vehicles. For example, steels which undergo a phase transformation during deformation, (i.e. Transformation-Induced Plasticity or TRIP steels) are promising candidates for these applications [1,2]. To achieve the desired room temperature mechanical properties, TRIP-aided steels undergo a complex annealing and cooling process where the critical step is the partial decomposition of austenite at low temperature. This phase transformation typically occurs in the temperature range of 300-500 °C.

The detailed mechanism of the bainite phase transformation remains one of the most controversial topics in physical metallurgy [3-7] with there being two opposing views. Proponents of the diffusional reaction mechanism [6-9] argue that the growth of bainitic ferrite occurs by the diffusion-controlled movement of ledges and that the carbon concentration of bainitic ferrite is in equilibrium with respect to austenite. Alternatively, assuming the displacive reaction mechanism [3,4,10] it is proposed that bainite forms without diffusion and that carbon subsequently redistributes or precipitates as carbides [3,11]. The situation is further complicated for alloys containing substantial additions of silicon because silicon suppresses or delays the formation of Fe₃C [3,12,13] by increasing the activity of carbon [14,15]. In this case, the terminology of carbide free bainite has been widely used although Hillert and Purdy [16] argue that this is a misuse of the term bainite and this transformation should be characterized as the growth of Widmanstätten plates. Finally, the

possibility exists that the mechanism changes depending on the transformation temperature and the detailed chemistry. Minote *et al.* studied the low temperature transformation behaviour of a TRIP steel (0.19 wt%C - 1.51 wt%Mn - 1.45 wt%Si), in which the evolution of bainite volume fraction was determined and compared to the model predictions based on diffusional and displacive mechanisms [17]. Their analysis suggests that the bainite transformation in this particular case follows the diffusional mechanism above 350 °C and the displacive mechanism below 350 °C.

It is not the purpose of this paper to attempt to answer these controversial questions. However, regardless of the mechanism, it is critical to understand the rate of transformation and its linkage to the redistribution of carbon during the reaction. Indeed, the redistribution of carbon controls the stability of austenite because the martensite start (M_s) temperature is strongly dependent on carbon concentration [18,19]. In order to preserve retained austenite at room temperature, the M_s temperature should be lower than room temperature. In addition, to obtain optimal mechanical properties, it is important to tailor the stability of retained austenite such that the deformation induced transformation of retained austenite to martensite occurs continuously during straining [20]. Although the low temperature decomposition of austenite has been extensively studied, there is a lack of knowledge regarding carbon redistribution since it is difficult to measure. Traditionally, dilatometry and metallography have been used to study the fraction transformed [21] but these techniques do not offer any information on carbon redistribution. Furthermore, dimensional changes from dilatometry measurements can arise due to both the phase transformation and carbon redistribution. Most commonly, the carbon concentration in retained austenite is determined by room temperature X-ray diffraction studies. However, there is considerable uncertainty in

the analysis as, for example, discussed by De Meyer et al. [22]. Recently, Babu et al.[23] have used an X-ray synchrotron source to conduct *in situ* measurements of transformation and carbon redistribution based on X-ray diffraction on a high carbon (0.75 wt%), high alloy steel. However, only a small volume of material could be examined in these experiments and care must be taken to avoid decarburization of the samples during the test.

1.2 Neutron BET Technique

Neutron Bragg-Edge Transmission (BET) technique is closely related to the neutron diffraction technique, i.e. both are related to the Bragg's law [24]:

$$\lambda = 2d_{hkl} \sin\theta \quad [(1)]$$

where λ is the wave length of the incident radiation, d_{hkl} is the lattice spacing of the crystal plane $\{hkl\}$ and θ is the diffraction angle. When an incident neutron beam with appropriate energy spectrum enters a crystalline sample, the intensity is split into three parts: i) the diffracted beam, ii) the scattered intensity and iii) the transmitted intensity. In the diffraction technique, the structural information is provided by the diffracted neutrons, which have a characteristic energy distribution. However, the majority of neutrons in the incident beam travel through the sample volume for most materials without being scattered. Therefore, the collected intensity for the diffracted neutron beam is low, which translates to longer data acquisition times in order to obtain good statistics. In addition, a fixed diffraction geometry must be maintained in the neutron diffraction setup, restricting the flexibility in controlling the sample temperature. On the other hand, there are benefits to examining the transmitted neutron beam from which the diffracted neutrons are missing. Since the intensity of the transmitted neutron beam is greater than that of the diffracted beam, higher time resolution

can be achieved with the transmission technique, compared to the conventional diffraction technique.

In a neutron BET experimental setup, the sample is placed in between the neutron source and the transmission detector. In contrast to a diffraction experimental setup, neutron source, sample and detector are located on a common axis. Due to the wave properties of neutrons, Bragg's law (equation [1]) is applicable when neutrons interact with crystalline solids. From this law it is clear that no radiation of a wavelength greater than $2d_{hkl}$ can be diffracted by a particular set of lattice planes $\{hkl\}$. Since the neutrons are emitted in pulses from the source and the neutron wavelength is proportional to the time of flight (TOF) between the source and the detector, the transmitted intensity rises abruptly at $\lambda = 2d_{hkl}$, forming a so-called Bragg-edge in the transmission spectrum at that wavelength. The height and width of a Bragg-edge follow the same laws as the intensity and width of a diffraction peak. Accordingly, a transmission spectrum contains in principle the same information as a conventional diffraction pattern, i.e. crystallographic structure, lattice parameter, volume fraction, etc. Most interestingly, for the study of steel phase transformations, the lattice parameter can be used to derive the carbon concentration information in the austenite and ferrite, as has been demonstrated by various researchers [25-27].

The attenuation (due to absorption and scattering) of neutrons in most materials is low enough to allow the transmission of a large fraction of the incident intensity through a sample of several millimeters (10-50 mm) in thickness. Also, beam spot sizes at neutron sources can be of the order of 10's of millimeters. Compared to transmission electron microscopy (TEM) or X-ray techniques, this allows one to probe relatively large sample volumes, on the order of cubic centimeters. In practice, the general application of the Bragg-

edge transmission technique is limited by the fact that small changes (edge-heights) of a large signal (transmitted intensity) have to be measured. This restricts Bragg-edge transmission experiments to systems of high symmetry (few reflections/edges) which consist of atomic nuclei with a high scattering length and low absorption cross-section, such as steel.

Previously, neutron BET technique has been applied for structural phase transformations [28-32] as well as strain measurement[33-35] at the spallation sources at Los Alamos Neutron Science Centre (LANSCE) and ISIS (located at the Rutherford Appleton Laboratory, near Oxford, UK). The work of Meggers *et al.* [36] demonstrated that a time resolution of 20 μ s is achievable in obtaining phase fractions and lattice parameters using a single pulse of neutron. Vogel [37] used the neutron BET neutron technique to study the low temperature decomposition of austenite in steel, however, the study suffered from poor temperature control on the sample. In a time-resolved kinetic phase transformation study, a large amount of neutron BET datasets can be generated in a single run, rendering manual data analysis rather low in efficiency. Practical data analysis involves software automation of the data processing procedure [38].

The current study demonstrates the potential of using a new technique based on the neutron (BET approach to making *in situ* measurements of the volume fraction of the FCC and BCC phase as well as the average carbon concentrations in the FCC phase.

2. *Experimental Methodology*

Neutron BET experiments were conducted on flightpath 5 at the (LANSCE)[39,40]. LANSCE has a pulsed neutron source (20 Hz) in which high flux neutrons are produced from a spallation source [41]. The flightpath consists of an evacuated beam tube of 6.73 m in length between moderator and the shielded experimental room (the “cave”), followed by a

second evacuated beam tube of 45.7 m in length leading to the detector station. The evacuation of both tubes (less than 50 Pa) prevents the intensity losses of 5% per meter which are found in dry air. Before entering the cave, a variable collimator made of alternating rings of polyethylene and steel with holes of converging diameter is installed next to the first tube to collimate the incident neutron beam. Neutrons exit the first tube through a 40 mm diameter hole in the last collimation ring into the cave where the facility for heat treatment is located. For the total flightpath, the distance between moderator and detector was 58.6 m. As it was not possible for users to be present in the cave when the neutron beam was present, the experimental apparatus was designed for operation by remote control.

In order to simulate the two-stage heat treatment required for the isothermal transformation studies, two tube furnaces were employed as shown schematically in Figure 1. The temperature of the first tube furnace (105 cm in length) was kept at 1000 °C while the second furnace (60 cm in length) was adjusted to a temperature between 275 and 450 °C. During the experiment, helium gas flowed through the furnaces at a rate of 1.5 l/min to minimize oxidation and decarburization of the samples. Between the two furnaces, a helium gas quench unit was placed so that the samples could be rapidly cooled from 1000 °C to the temperature of the second furnace. The quench unit consisted of a 6.35 mm square spray nozzle, a diameter of 76.2 and length of 150 mm funnel to guide the gas to the sample and a remote controlled solenoid valve and tubing. The gas pressure was adjusted to 275 kPa during quenching and the cooling time interval was pre-determined in such a way that the sample temperature loss leaving the quench zone was within about 5 °C of the second furnace. A sample manipulator was designed to move the sample assembly at a speed of 0.12 m/s between the furnaces and the quench unit. Before starting the experiments, the

furnaces, the quench unit and the sample manipulator were aligned with the help of a laser beam so that the centre region of the sample was covered by the neutron beam (40 mm in diameter). Runs without the sample confirmed that the transmission signal was free of contamination from the sample environment.

The steel used in these experiments had a nominal chemical composition of 0.4C - 3Mn - 2Si (in wt%) and was chosen since a previous study by Bhadeshia and Edmonds [10] had shown that the time scale for the low temperature transformation was approximately 2 hours, i.e a convenient time to demonstrate the feasibility of the BET technique. In addition, the high silicon level in this steel should considerably retard the formation of Fe₃C precipitates making the analysis of the data simpler, i.e. Bhadeshia and Edmonds found no evidence for carbide precipitation even after 74 h at 350 °C [10].

The steel was produced in two batches with the chemical compositions shown in Table 1. There is a slight variation in the chemistry but this was not considered significant for the present study. The steel was cast to a 80 kg ingot, and was then hot-rolled to sheets of 60mm in width and 1.6 mm in thickness. After removing the surface oxide formed during hot-rolling, the sheet samples were machined to disks 55 mm in diameter and approximately 1 mm thickness.

The geometric design of the samples for experiments was an important consideration for the current study. The magnitude of the Bragg edges increases with the volume of material tested and requires a minimum thickness of steel which is approximately 10-15 mm. At the same time, the use of a large sample potentially introduces an inhomogeneous temperature distribution during the quench process. To overcome these competing considerations, samples for the neutron BET experiments were assembled as stacks of disks as shown in

Figure 2. Two stainless steel rings connected by long bolts form the frame in which 15 sample disks were fixed in the right positions by the bolts and separated by 1.5 mm thick stainless steel washers. The sample assembly was designed so that the sample disks were not constrained by the frame and no stress was developed during the applied thermal cycle. The stainless steel rings which held the sample in place had an inner diameter of 45 mm thus leaving suitable clearance for the 40 mm diameter collimated neutron beam to pass through without sampling the rings. A run with the frame in place but without the steel disks showed no Bragg-edges from the frame material.

The temperature of the sample during the experiment was measured using a type K thermocouple spot-welded to the centre of the central disk in the sample assembly. For selected experiments, extra type K thermocouples were attached to the edges of the centre disk, as well as in the centre of the disks other than the central disk to examine the homogeneity of sample disk temperature in the assembly with the results shown in Table 2. The greatest temperature difference observed was 7 °C between the top and bottom edge of the centre disk at a sample temperature of 1000 °C which falls within the limits of error for K-type thermocouples. It was, therefore, concluded that the temperature distribution in the sample disks was essentially homogeneous.

The sequence for conducting an experimental run was as follows: The sample assembly was loaded in the centre of the first furnace and then helium gas flow was initiated. The neutron cave was then swept and the neutron shutter was opened to allow the neutron beam to pass through the sample disks. The sample temperature was raised to the austenitization temperature of 1000 °C and held for 30 minutes resulting in an average austenite grain size of 110 µm, as measured by optical microscopy of prior austenite grain boundaries. The sample

assembly was then moved into the quench unit where it was cooled rapidly by the helium gas. When the target temperature was reached, the sample assembly was moved from the quench unit into the second tube furnace, which had been preheated and held at the transformation temperature. The sample stayed at the transformation reaction temperature for up to 10 hours before it was finally removed from the furnace and quenched to room temperature. The thermal cycles applied to the material are summarized in Table 3. An example of the recorded experimental thermal cycle is given in Figure 3. For 1000 °C/335 °C and 1000 °C/400 °C run cycles, materials from batch A were used. For all other run cycles, materials from batch B were used.

The transmitted neutron beam intensity vs. time-of-flight was integrated over 5 s intervals. The data read-out and storage required another 7 s, thus, a total of 12 seconds is required for a single data acquisition cycle. Neutron patterns were recorded for 4 to 10 hours such that the entire transformation could be examined. For a single experimental run, the number of transmitted neutron patterns generated ranges from 1900 to 2700 patterns, depending on the duration of the experiment. The data analysis was based on a full pattern fitting against a model which uses the Rietveld approach [42]. Phase volume fraction information can be extracted from the Bragg edge height parameter, lattice parameter information can be extracted from the edge position, and edge width parameter can be obtained from the edge profile. The details of the analysis software is published in the literature [37,38]. The d-spacing range used for these experiments was 0.05 to 0.16 nm, resulting in 13 reflections from planes of the BCC ferrite lattice and 15 reflections from the planes of the FCC austenite lattice, respectively. The starting values for a BET pattern were the fit parameters of the previous pattern. The analysis was deemed successful if the

parameter curves vs. time (volume fractions, lattice parameters) agreed within statistical errors for chronologically forward and reverse analysis.

In order to examine the validity of the analysis for volume fraction determination, a series of measurements were conducted at room temperature by using a sample made by stacking 15 plates of interstitial free steel and 304 stainless steel. The IF steel plates were 50.4 x 50.4 x 0.655 mm in size consisting of 100% ferrite (BCC) phase whereas the 304 stainless steel plates are of the dimensions 50.4 x 50.4 x 0.794 mm possessing 100% austenite (FCC) phase. By changing the number of IF steel and stainless steel plates, the volume fraction of the BCC phase in the sample assembly was changed in a systematic manner.

After the heat treatment cycle, selected samples were measured using XRD at room temperature in a Siemens D5000 diffractometer to obtain the phase volume fraction in order to compare with the final volume fractions from the neutron BET results. The XRD sample of 1.25 cm² was cut and polished, in the final step by using 1 μm diamond paste. The experimental parameters for the XRD step scan were as follows: Cu K_α radiation, 40 kV, 30 mA, 2θ scanning range: 40° to 85°, step size: 0.01 ° and dwell time 1 s. The XRD data were analyzed using the Rietveld approach[42] and the GSAS (General Structural Analysis System) program [43] in order to obtain the austenite and ferrite volume fractions.

Microstructure of the sample was also characterized using conventional optical metallography. The etching was carried out by swabbing the sample with 2 % Nital for 3 seconds, rinsing in water, followed by immersing the sample in 10 % sodium meta-bisulfite aqueous solution for 15 seconds. Quantitative volume fraction analyses were done on selected samples using the Clemex imaging analysis system.

In order to test whether the cooling rate was above the critical value to avoid a phase transformation when the sample was transferred from the first furnace temperature at 1000 °C to the second furnace temperature, dilatometer experiments were conducted on a Gleeble 1500 thermo-mechanical simulator. A steel sample of $60 \times 12 \times 1.2 \text{ mm}^3$ in size for the as-received condition was given the same thermal treatment as the neutron BET runs, i.e. 1000 °C/30 min followed by controlled cooling at 6 °C/s to room temperature, i.e. at the minimum cooling rate recorded during the neutron BET runs. Finally, one of the neutron BET experiment runs (1000 °C/335°C) was also replicated using the Gleeble 3500 Thermomechanical simulator. Dilatometry data was acquired and analyzed to determine the transformation kinetics independent of the BET experiments.

3. Results

3.1 BET Experiments

Figure 3 shows the experimentally determined and recorded temperature-time history for the sample where the low temperature decomposition of austenite occurred at 355 °C. The cooling rate between the austenization and the austenite decomposition temperatures was in the range of 6 to 16 °C/s and was found to be similar for all experiments. The dilatometry results for cooling at 6 °C/s (i.e the minimum cooling rate) showed that there was no evidence of a phase transformation at this cooling rate and therefore it was assumed that the cooling rate was sufficiently high to avoid ferrite formation. Thus, the starting structure for the transformation at low temperatures was assumed to be 100 % FCC phase (austenite).

Figure 4 illustrates a typical neutron transmission pattern (where the overall shape of the curve reflects the energy distribution of the neutron beam. Superimposed on this distribution are the Bragg edges where the neutron intensity is increasing with increasing TOF due to

exclusion of the particular set of lattice planes from the diffraction process. The overall pattern will be subsequently referred to as a Bragg edge transmission (BET) pattern. The insets in Figure 4 illustrate an expanded view for the edges which result from the (321) planes of the BCC structure and the (311) planes in the FCC crystal structure. It is possible to determine three parameters from each edge, i.e. the edge position which corresponds to the lattice parameter of the phase, the height of the edge which is related to the relative volume fraction of the phase (after correction for the crystallographic structure factor) and the edge width which is analogous to peak broadening in conventional X-ray diffraction analysis.

Figure 5 shows a time sequence of the BET patterns for a sample isothermally transformed at 335 °C for 0 to 8 hours. It can be observed that as time progresses the height of BCC edges, (e.g. the (321) edge highlighted on the figure), increases while the height of the FCC edges (e.g. the (311) edge) decreases. From this sequence, it is possible to follow the evolution of the volume fraction, the FCC and BCC lattice parameters and the edge width parameter for the FCC phase as a function of time as shown in Figure 6 for an isothermal experiment at 335 °C. Figure 6a illustrates that for the same heat treatment as shown in Figure 5, the low temperature BCC phase increases in volume fraction from near zero at the beginning of the experiment to a plateau value of 65% after 2-3 hours. Thereafter, there is no observed change in the relative volume fraction. Figure 6b corresponds to the evolution of the lattice parameter for the FCC and BCC phases as a function of the transformation time. In this case, the variation of the BCC lattice parameter shows only a very small change (i.e. within the limits of measurement errors) while the FCC lattice parameter increases from 0.3615 to 0.3655 nm. The change in the FCC lattice parameter follows closely the change in volume fraction of the FCC phase which will be discussed in the following sections. Finally,

both the edge width parameter and its scatter observed systematically increases as the transformation progresses.

Figure 7a provides a summary of the transformed volume fractions of the BCC phase as a function of the isothermal annealing temperature and time. No evidence for the formation of the BCC phase was detected at 436 °C. For the other transformation temperatures, the maximum volume fraction of the BCC phase formed during the transformation increases with decreasing temperature. The Bragg edge width parameter which can be considered as a measure of material inhomogeneity increases with the fraction transformed at the temperatures of 283, 335 and 355 °C, see Figure 7b.

The morphology of the transformed phases at the end of the isothermal annealing period was evaluated using optical metallography. Figure 8 shows the microstructures observed at different transformation temperatures at 283, 335 and 405 °C and time intervals of 9, 8 and 6 hours, respectively. For the sample transformed at 283 °C (Figure 8a), one observes an acicular structure composed of fine ferrite (BCC) and a smaller fraction of retained austenite islands. Analysis of room temperature X-ray diffraction data reveals an austenite volume fraction of 19 ± 0.7 %. As the transformation temperature is raised the microstructure becomes coarser. Figure 8b shows the final microstructure for a sample held for 8 hours at 335 °C. Metallography reveals three distinct phases (ferrite appears as dark grey, austenite shows a white colour austenite and martensite is brown). The ferrite packets are considerably coarser at this temperature compared to 283 °C. Quantitative metallography reveals that the fraction of this phase was determined to be 61 ± 2 %. Figure 8c, illustrates the microstructure transformed at 405 °C for 6 hours. In accordance with the preceding description, the dark grey phase is the ferrite phase, however, in this case, due to different

etching conditions, the white phase is martensite. The total fraction of the ferrite phase was measured to be 25 ± 3 % by quantitative metallography.

3.2 Validation of BET Technique

3.2.1 Volume fraction

The volume fraction of the different phases can be determined from an analysis of the relative edges. In order to validate this analysis, a series of measurements were conducted on samples where the number of FCC and BCC plates was systematically varied to change the volume fraction as described in Section 2 and Figure 9 shows the results. It can be seen that for BCC volume fractions in the range of approximately 5 to 95%, the measured values agree well with the true values, although these are systematically about 3% higher than the true volume fractions. This may be attributed to the texture that may exist in the sample material or to the high chromium and nickel contents in the 304 stainless steel which may affect the scattering of neutrons. For BCC volume fractions of 0 and 100%, the analysis gives a result which was negative and greater than 100%, respectively. This happens when the data analysis software is forced to fit both BCC and FCC edges on the pattern obtained from samples where only one phase is present. The occurrence of some noise in the BET pattern leads to non-zero values for the non-present phase. Thus, it is concluded that phase fractions derived from BET patterns are reliable to within 3 % in the range of 5% to 95% of the transformed austenite.

In addition to these experiments, it was possible to compare the BET results with those obtained using other techniques, e.g. X-ray diffraction, for the final microstructures of the samples after the low decomposition of austenite. Table 4 summarizes results from X-ray diffraction, optical metallography and the BET experiments. It can be observed that for the

transformation temperature of 283 °C, there is good agreement between the BET and X-ray diffraction results (it was not possible to conduct quantitative analysis of the optical microstructures in this case due to their complexity). After 1 hour annealing at the transformation temperature of 335 °C, the results of optical metallography show slightly lower volume fractions than determined by BET while after 8 hours annealing, the BET results are slightly lower than those determined by X-ray diffraction and metallography. For the transformation at 405 °C, the metallography and BET results are in agreement. It should be noted that X-ray diffraction results were not possible for this case because the austenite transformed to martensite during cooling of the sample and it was not possible to distinguish ferrite and martensite in the X-ray diffraction experiments. By considering the errors in measurement, all results are within the measurement accuracy with one exception of the results from X-ray diffraction and BET for transformation at 335 °C for 8 hours where the volume fractions determined by X-ray diffraction results were greater than those of the BET measurements. In this case, it is possible that there was the formation of some martensite upon cooling resulting in a larger volume fraction estimated for the BCC phase determined by the X-ray measurements.

3.2.2 Lattice Parameter

To examine the consistency of the data for the lattice parameter measurements, the value of the lattice parameter determined for the FCC phase at the beginning of the low temperature annealing period are plotted as a function of temperature as shown in Figure 10a. At the starting point, the lattice structure is 100 % of the FCC phase where the carbon is completely dissolved in the lattice. The slope of the lattice parameter vs. temperature curve

is a measure of the coefficient of thermal expansion (CTE) for this phase, i.e. $\alpha_{FCC} = \frac{\Delta a_{\gamma}}{a_{\gamma} \Delta T}$.

From the experimentally obtained neutron data, the CTE was determined to be $22.3 \times 10^{-6} \text{ K}^{-1}$ which agrees well with literature data of $22.8\text{-}23.2 \times 10^{-6} \text{ K}^{-1}$ for austenite of similar compositions reported by Onink et al. [26]. Figure 10b shows the lattice parameter of BCC iron measured in the final transformation stage, indicating a thermal expansion coefficient for ferrite of $14.7 \times 10^{-6} \text{ K}^{-1}$ consistent with the data summarized by Zhao et al. [44].

3.2.3 Transformation Kinetics

Figure 11 shows a comparison of the bainite transformation kinetics at $335 \text{ }^\circ\text{C}$ measured by neutron BET and dilatometry techniques. The dilatation data was analyzed using the method described in [44] and since the transformation was incomplete, it was necessary to fix the final fraction transformed. This was conducted by selecting a volume fraction 61 % as the final fraction which was obtained from quantitative image analysis. Generally, it can be observed that there is good agreement for the results obtained by the analysis of dilatometer and BET patterns, although the fraction transformed estimated from the dilatometer data is slightly larger in the range of 20-50% transformed. However, it is worth noting that dilatometry experiments measure both the length change due to phase transformation and due to lattice parameter changes from the redistribution of carbon, whereas BET de-couples the two values and shows only the volume fraction.

4. Discussion

It has been demonstrated that the results from the analysis of the BET patterns are reliable and then the overall transformation kinetics can be summarized by the temperature-time-transformation (TTT) diagram as shown in Figure 12. Assuming that 5 vol% transformed is a measure of the start of the reaction, the nose of the curve occurs in the temperature range of $350\text{-}400 \text{ }^\circ\text{C}$ which is consistent with the results from Bhadeshia and

Edmonds for a similar steel composition [10]. However, the incubation time measured in this work is 2-3 times greater than that reported by Bhadeshia and Edmonds which may be related to the challenges they faced in determining the fraction transformed from dilatometry measurements. It should be noted that a considerable uncertainty was reported in their work. This again underlines one important advantages of the BET technique because the effects of carbon redistribution and volume fraction transformed are decoupled, unlike dilatometry measurements. The dashed line at the top of Figure 12 is an empirical estimate for the start of the bainite transformation using the relationship proposed by Steven and Hayes [45] and it is found to be in good agreement with the current experimental results, i.e. no bainite formation at 436 °C was detected in the current work.

The carbon concentration in the FCC and BCC phases was established by relating the results of the lattice parameter measurements to the temperature and carbon dissolved in the lattice. It is assumed that the change in lattice parameter is dependent only on the carbon concentration and temperature, i.e. the effect of any possible redistribution of substitutional elements is considered negligible [46,47]. A quantitative relationship for the lattice parameter of FCC (austenite) phase can be expressed as:

$$a_{\gamma}(x_C^{\gamma}, T) = (a_{\gamma_ref} + \beta_{\gamma} x_C^{\gamma}) [1 + \alpha_{FCC} (T - T_{ref})] \quad (2)$$

where a_{γ} is the austenite lattice parameter, a_{γ_ref} the austenite lattice parameter for zero carbon concentration at the reference temperature T_{ref} , β_{γ} is a constant, x_C^{γ} is the carbon concentration in austenite and α_{γ} is the coefficient of thermal expansion of austenite. The value for the coefficient of thermal expansion for the austenite ($22.3 \times 10^{-6} \text{ K}^{-1}$) was taken from the experimentally determined temperature dependence of the lattice parameter (see Section 3, Figure 10a). The reference temperature was chosen to be 20 °C. Equation (2)

possesses two unknown quantities, i.e. the reference lattice parameter, $a_{\gamma_{ref}}$, and the value of β_{γ} . Most of the published data for β_{γ} [24,48-50] which are summarized in reference [22] suggest a value of 0.044 is appropriate. Thus, the only unknown quantity in applying equation (2) comes from the value of $a_{\gamma_{ref}}$. In the present case, the value of $a_{\gamma_{ref}}$ was determined by fitting the data taken at early stage of the low temperature annealing period prior to the phase transformation when the carbon concentration of austenite is 0.4 wt %. The lattice parameter was determined to be, $a_{\gamma_{ref}} = 0.3571$ nm. The important point to emphasize in this analysis is that the value of $a_{\gamma_{ref}}$ can be determined from a known carbon concentration, in this case 0.4 wt %. This will eliminate the considerable uncertainty of X-ray diffraction studies on retained austenite at room temperature [22]. As an example of the conversion, Table 5 reports the experimental data for the lattice parameters of the FCC phase possessing different carbon concentrations for selected transformation conditions and the determined average carbon concentrations.

The evolution of the carbon concentration in the FCC phase as a function of the transformed volume fraction is plotted in Figure 13 for isothermal annealing at 283, 335, 355 and 405 °C. It is shown that the data for all temperatures are represented by one single curve which is consistent with conducting a mass balance on the carbon presented as the dashed line. These results are in good agreement with those of Bhadeshia and Edmonds who reported that the relatively high silicon level in this steel postpones carbide precipitation [10], i.e. the carbon atoms are either in the austenite or ferrite lattices. The collapse of the data onto a single curve provides a further consistency check for the current experimental technique.

It also is apparent that the Bragg edge width parameter is useful for characterizing the material inhomogeneity but, its interpretation is non-trivial. As mentioned earlier, the edge width parameter is analogous to the peak width in conventional diffraction experiments. Therefore, the increase in the edge width can be related to factors which cause peak broadening such as chemical inhomogeneity, the presence of internal stresses and increased dislocation density. It is therefore difficult to attribute the increase in the Bragg edge width parameter to a single effect. Further work is required in order to conduct a quantitative analysis of the determined parameters.

5. Summary

The current work demonstrates a novel approach by using the neutron Bragg edge transmission technique to measure *in situ* the low temperature phase transformation in medium carbon steels. The following are the significant specific results of this work:

1. It is possible to measure the volume fraction transformed and the lattice parameters of the phases achieving a time resolution of approximately 10 s. The lattice parameter is a measure estimate the average carbon concentration in the austenite phase. The significant advantage that the analysis is self-consistent based on the initial measurement of the austenite lattice parameter when 100 vol% austenite is present. In addition another advantage of this technique is to determine the lattice parameters and transformed volume fractions of the coexisting phases compared to post transformation X-ray diffraction measurements conducted at room temperature. In addition, BET allows for measurement of carbon concentration and volume fraction independently, whereas, for example, dilatometry provides a convolution of these two quantities.

2. The results show that for a medium carbon steel with approximately 2 wt% silicon, carbide precipitation is not detected consistent with previous results. The redistribution of carbon in the austenite phase is consistent with the mass balance. The data obtained for carbon enrichment can be represented by a single master curve.
3. The edge width parameter can be used as a measure of material inhomogeneity, although similar to X-ray peak broadening, it is difficult to deconvolute the various effects of chemical inhomogeneity, internal stresses, dislocation density gradients and size effects. This requires further work to clarify the dominant effect(s).

The validity of the neutron BET measurements to determine phase transformation parameters and to quantify carbide precipitation in silicon containing TRIP steels has been demonstrated. Furthermore, improvements in the experimental technique can be conducted (e.g. increased sampling rate, higher beam currents, better data acquisition and analysis). This will allow for the examination of leaner steel compositions of commercial interest where the phase transformation is much faster.

Acknowledgements

The financial support from the Natural Sciences and Engineering Research Council of Canada (NSERC) is gratefully acknowledged. The neutron Bragg-edge transmission work has benefited from the use of the Los Alamos Neutron Science Centre (LANSCE) at the Los Alamos National Laboratory (LANL). This facility is funded by the US Department of Energy under Contract W-7405-ENG-36. One of the authors (J. Huang) is also grateful for

the travel assistance from the STONE program made available through the Los Alamos National Laboratory's University of California Directed Research and Development Office (UCDRD) and LANSCE Division. Finally, the financial support of the FNRS (Belgium) to cast and fabricate the material is gratefully acknowledged.

REFERENCES

- [1] Ushioda, K. *Scand. J. Metall.* 1999;28:33.
- [2] De Meyer, M., De Cooman, B.C., Vandershueren, D. *Iron and Steelmaker* 2000;27:55.
- [3] Bhadeshia, H.K.D.H., In: *Bainite in Steels*; Institute of Materials, London, UK;1992.72.
- [4] Bhadeshia, H.K.D.H., Christian, J.W. *Metall. Trans. A.* 1990;21A:767.
- [5] Aaronson, H.I., Reynolds, W.T.J., Shiflet, G.J., Spanos, G. *Metall. Trans.* 1990;21A:1343.
- [6] Hehemann, R.F., Kinsman, K.R., Aaronson, H.I. *Metall. Mater. Trans.* 1972;3:1077.
- [7] Purdy, G.R., Hillert, M. *Acta metall.* 1984;32:823.
- [8] Reynolds, W.T.J., Aaronson, H.I., Spanos, G. *Materials Transactions, JIM (Japan)*. 1991;32: 737.
- [9] Hillert, M. *Scr. Mater.* 2002;47:175.
- [10] Bhadeshia, H.K.D.H., Edmonds, D.V. *Metall. Trans. A.* 1979;10A:895.
- [11] Christian, J.W., In: *Theory of Transformations in Metals and Alloys*; 3rd ed.; Pergamon Press, London, UK; Part II;2002.
- [12] Tsukatani, I.H., S I; Inoue, T *ISIJ Int.* 1991;31:992.
- [13] Honeycombe, R.W.K., Bhadeshia, H.K.D.H., In: *Steels: Microstructures and Properties*; Edward Arnold, London, UK;1995.103.
- [14] Darken, L.S. *Trans. AIME* 1949;180:430.
- [15] Owen, W.S. *Trans. ASM* 1954;46:812.
- [16] Hillert, M., Purdy, G.R. *Scr. Mater.* 2000;43:831.
- [17] Minote, T., Torizuka, S., Ogawa, A., Niikura, M. *ISIJ Int.* 1996;36:201.
- [18] Andrews, K.W. *J. Iron Steel Inst.* 1965;203:721.
- [19] Kung, C.Y., Rayment, J.J. *Metall. Trans.* 1982;13A:328.
- [20] Itami, A., Takahashi, M., Ushioda, K. *ISIJ Int.* 1995;35:1121.
- [21] Jacques, P., Eberle, K., Harlet, P., Delannay, F. In: *40th Mechanical Working and Steel Processing Conference*; Iron and Steel Society/AIME; 1998; p.239.
- [22] De Meyer, M., Vandershueren, D., De Blauwe, K., De Cooman, B.C. In: *41st Mechanical Working and Steel Processing Conference*; Iron and Steel Society/AIME; 1999; Vol. XXXVII; p.483.
- [23] Babu, S.S., Specht, E.D., David, S.A., Karapetrova, E., Zschack, P., Peet, M., Bhadeshia, H.K.D.H. *Metall. Mater. Trans.* 2005;36A:3281.
- [24] Cullity, B.D., In: *Elements of X-ray Diffraction*; Addison-Wesley, New York, NY;1978.508.
- [25] Reed, R.C., Akbay, T., Shen, Z., Robinson, J.M., Root, J.H. *Mat. Sci. Eng. A* 1998;A256:152.
- [26] Onink, M., Brakman, C.M., Tichelaar, F.D., Mittemeijer, E.J., van der Zwaag, S., Root, J.H., Konyer, N.B. *Scr. Metall. Mater.* 1993;29:1011.
- [27] Huang, J., Hammond, R.P., Conlon, K., Poole, W.J. In: *Int. Conf. on TRIP-Aided High Strength Ferrous Alloys*; De Cooman, B.C., Ed.; Wissenschaftsverlag Mainz GmbH; 2002; p.187.

- [28] Meggers, K., Priesmeyer, H.G., Trela, W.J., Bowman, C.D., Dahms, M. Nucl. Instrum. Methods Phys. Res. B. 1994;88:423.
- [29] Meggers, K., Priesmeyer, H.G., Trela, W.J., Dahms, M. Mat. Sci. Eng. A 1994;188:301.
- [30] Bourke, M.A.M., Maldonado, J.G., Masters, D., Meggers, K., Priesmeyer, H.G. Mat. Sci. Eng. A 1996;221:1.
- [31] Stalder, M., Vogel, S., Bourke, M.A.M., Maldonado, J.G., Thomas, D.J., Yuan, V.W. Mat. Sci. Eng. A. 2000;280:270.
- [32] Vogel, S., Ustundag, E., Hanan, J.C., Yuan, V.W., Bourke, M.A.M. Mat. Sci. Eng. A. 2002;A33:1.
- [33] Santisteban, J.R., Edwards, L., Steuwer, A., Withers, P.J. J. Appl. Cryst. 2001;34:289.
- [34] Steuwer, A., Withers, P.J., Santisteban, J.R., Edwards, L., Bruno, G., Fitzpatrick, M.E., Daymond, M.R., Johnson, M.W., Wang, D. Phys. Stat. Sol. A 2001;185:221.
- [35] Santisteban, J.R., Edwards, L., Priesmeyer, H.G., Vogel, S. App. Phys. A: Mat. Sci. Process. 2002;74:S1616.
- [36] Meggers, K., Priesmeyer, H.G., Stalder, M., Vogel, S., Trela, W. Physica B 234: 1160-1162 1997;234.
- [37] Vogel, S. Ph.D. Thesis, Universität Kiel, Germany; 2000.
- [38] Vogel, S., Priesmeyer, H.G. Advances in X-ray Analysis 2001;44:91.
- [39] Lisowski, P.W., Bowman, C.D., Russell, G.J., Wender, S.A. Nucl. Sci. Eng. 1990;106:208.
- [40] Roberts, J.A. Neutron News 1999;10:11.
- [41] Windsor, C.G., In: Pulsed neutron scattering; 1st ed.; Taylor and Francis, London, UK;1981.
- [42] Rietveld, H.M. J. Appl. Cryst. 1969;2:65.
- [43] Larson, A.C., von Dreele, R.B. General Structure Analysis System (GSAS), Los Alamos National Laboratory Report LAUR 86-748, 2004.
- [44] Zhao, J.Z., Mesplont, C., De Cooman, B.C. Mat. Sci. Tech. 2002;18:1115.
- [45] Steven, W., Hayes, A.G. J. Iron Steel Inst. 1956;183:349.
- [46] Stark, I., Smith, G.D.W., Bhadeshia, H.K.D.H. Metall. Trans. A. 1990;21A:837.
- [47] Hall, D.J., Bhadeshia, H.K.D.H., Stobbs, W.M. J. de Physique IV 1982;43:449.
- [48] Zhang, M.-X., Kelly, P.M. Mat. Char. 1998;40:159.
- [49] Ruhl, R.C., Cohen, M. Trans. Met. Soc. AIME 1969;245:241.
- [50] Hanzaki, A.Z., Hodgson, P.D., Yue, S. ISIJ Int. 1995;35:324.

Tables

Table 1 Chemical composition of the steel (wt. %).

Steel	C	Mn	P	S	Si	Cu	Ni	Cr	Mo	V	Nb	N	B	Ti	Al*
Batch A	.43	3.08	.008	.001	2.19	.006	.015	.017	.002	.002	.002	.004	.0004	.002	.002
Batch B	.38	2.99	.016	.002	1.95	.006	.018	.021	.002	.002	.002	.005	.0002	.005	.042

* Acid Soluble Aluminium.

Table 2 Measured temperature homogeneity measurement in the sample disks.

Furnace Temperature	Disk Upper Edge Temperature	Disk Lower Edge Temperature	Disk Centre Temperature
1000 °C	1001 °C	995 °C	1002 °C
350 °C	353 °C	355 °C	347 °C
330 °C	334 °C	338 °C	338 °C

Table 3 Chosen heat treatment parameters for the material.

Austenitization Condition	Bainite Transformation Temperature °C
1000 °C /30 min.	283
	335
	355
	400
	405
	436

Table 4 Volume fraction of ferrite or BCC phase determined by from various techniques (BET, XRD and quantitative metallography).

Transformation condition	Neutron BET, %	XRD, %	Metallography, %
283 °C/9 hr.	80 ± 1.5	81 ± 0.7	-
335 °C/1 hr.	64 ± 1.5	-	61 ± 2
335 °C/8 hr.	70 ± 1.5	75 ± 0.6	72 ± 3
405 °C/5.8 hr.	25 ± 1.5	-	25 ± 3

Table 5 Summary of the FCC lattice parameter at the end of the BET run and the calculated carbon concentration for the various transformation conditions.

Transformation condition	Retained austenite lattice parameter nm	Calculated carbon concentration wt%
283 °C/9 hr.	0.36858	2.11
335 °C/1 hr.	0.36408	1.07
335 °C/8 hr.	0.36518	1.30
405 °C/5.8 hr.	0.36249	0.55

Figures

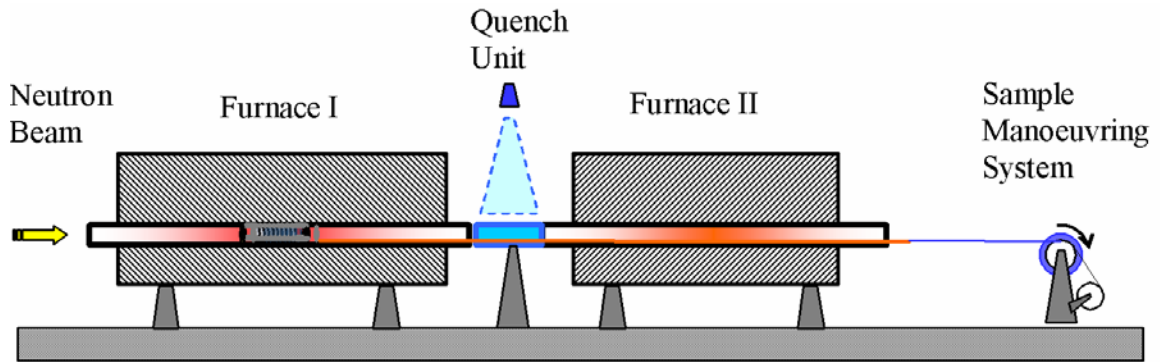


Figure 1 Schematic illustration of the experimental set-up used in the neutron BET experiment. Furnace I was held at the austenization temperature of 1000 °C and furnace II was controlled at temperatures between 283 and 436 °C.

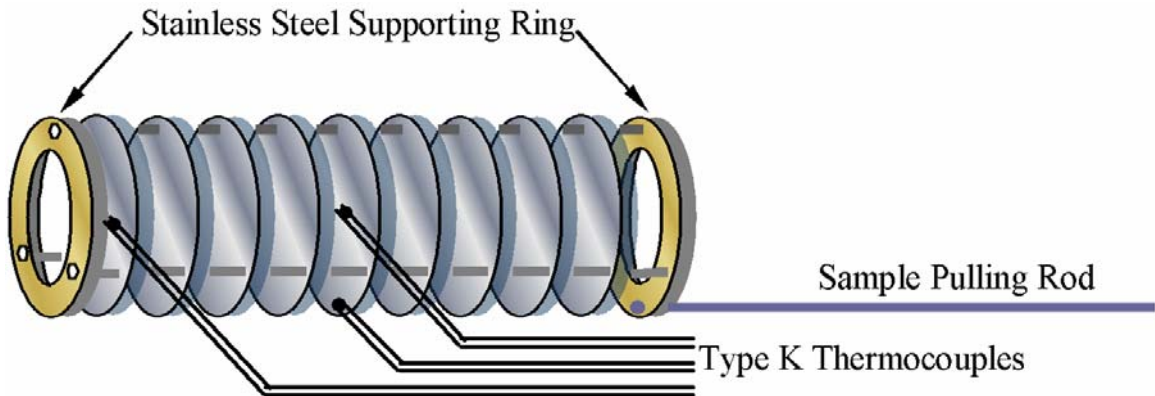


Figure 2 Schematic illustration of the sample assembly used for the neutron BET experiment. The distance of the sample assembly between the supporting rings is approximately 60 mm.

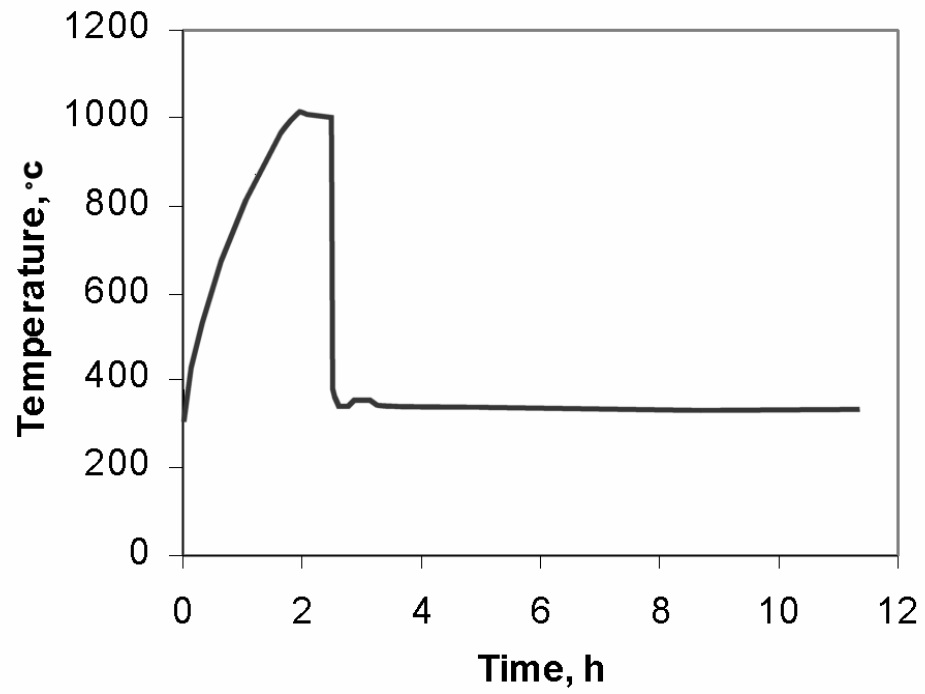


Figure 3 Temperature vs. time curve representing an example of the experimentally measured thermal cycle applied to the steel. The temperature was measured in the centre of the middle disk as shown in Figure 2.

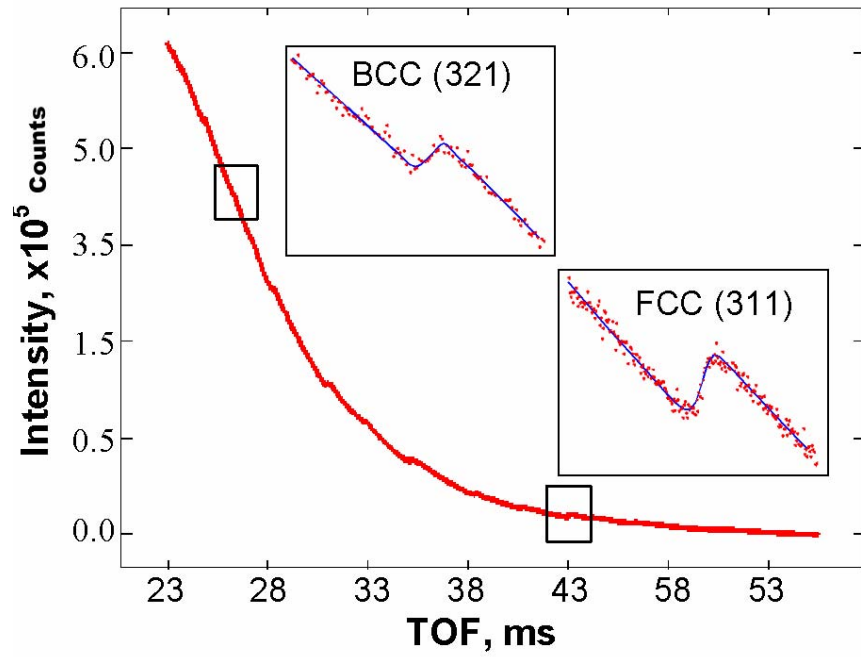


Figure 4 Neutron BET pattern of a sample isothermally transformed at 335 °C after 45 minutes shows the edge of the (321) for the BCC lattice and the (311) edge for the FCC lattice.

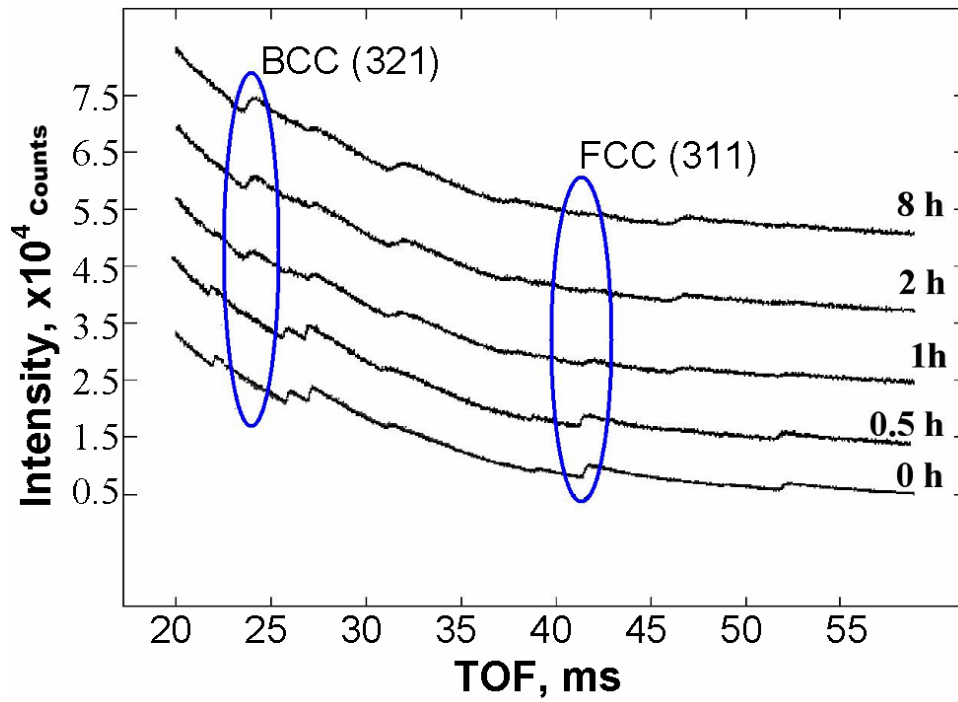
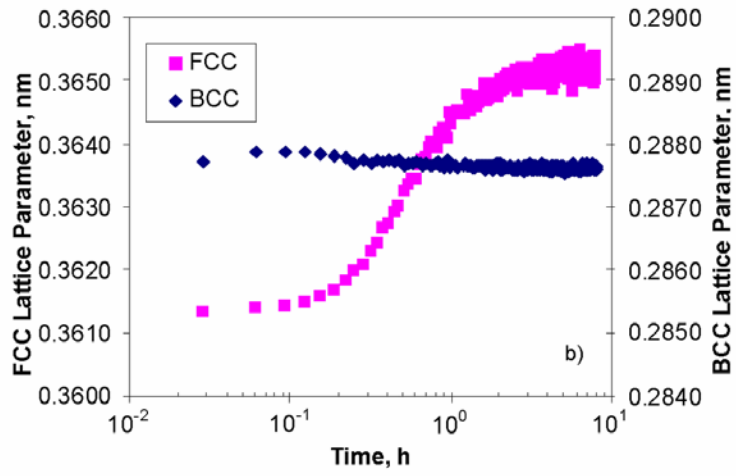
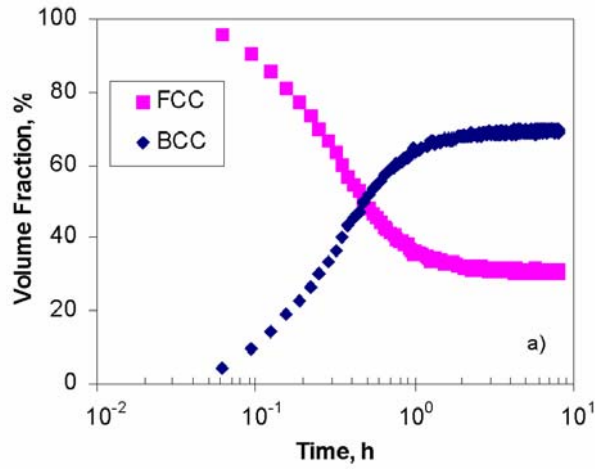


Figure 5 Neutron BET patterns obtained for a steel sample isothermally transformed at a decomposition temperature of 335 °C, after austenization at 1000 °C for 30 min.



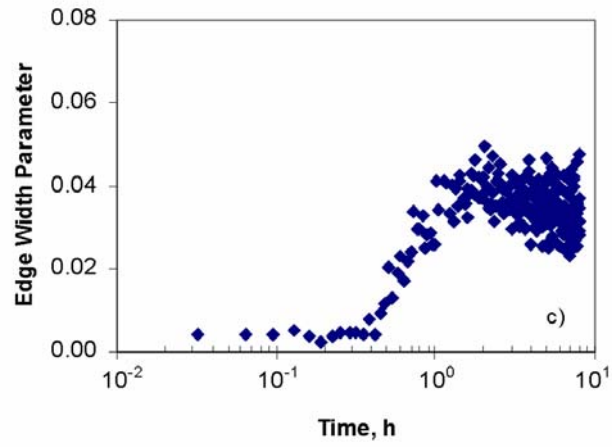
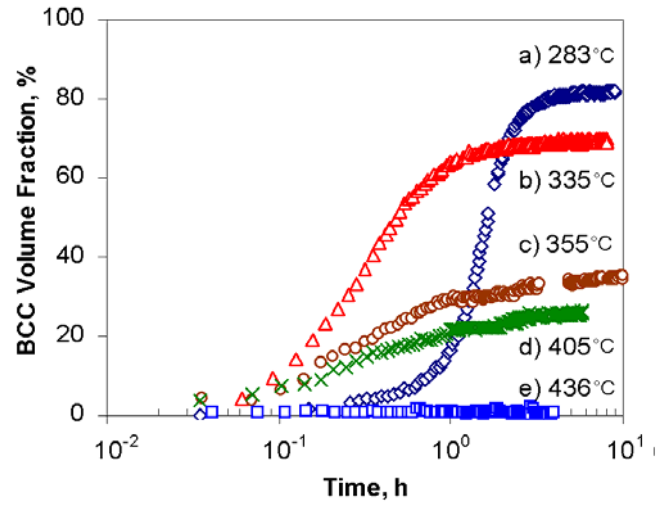
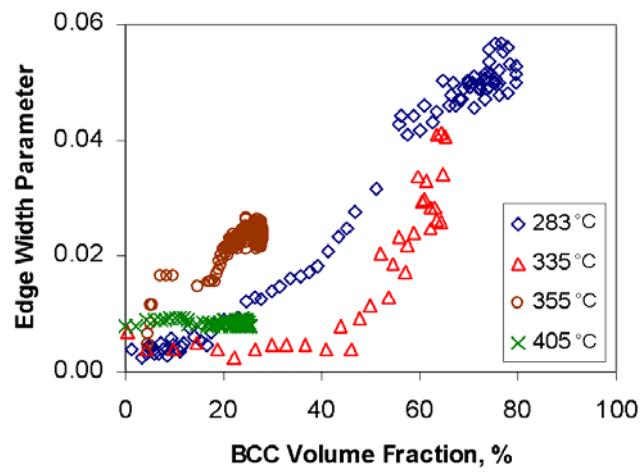


Figure 6 Results obtained from the data analysis for the same heat treatment shown in Figure 5: a) time dependent evolution of the volume fraction of FCC and BCC phases, b) lattice parameters of the FCC and BCC phases and c) edge width parameter for austenite.

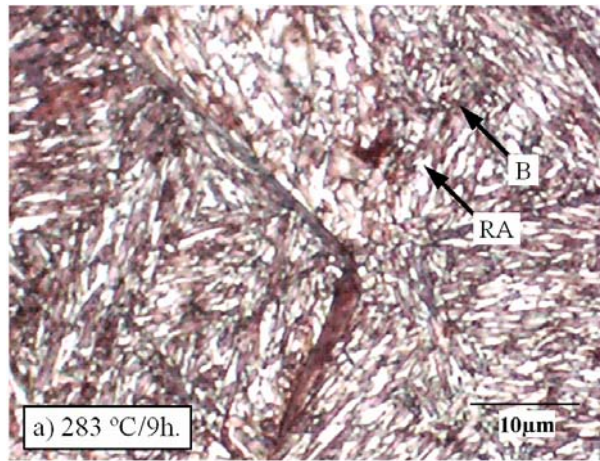


(a)

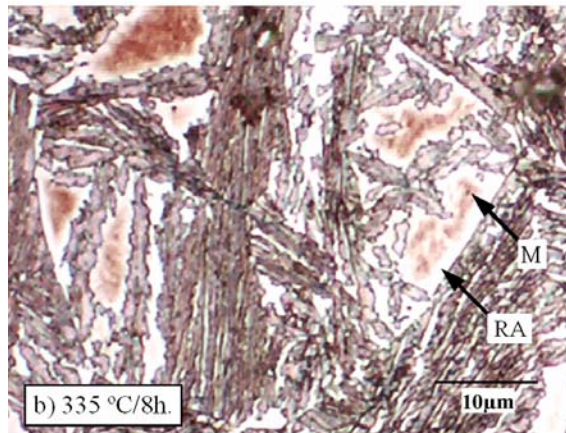


(b)

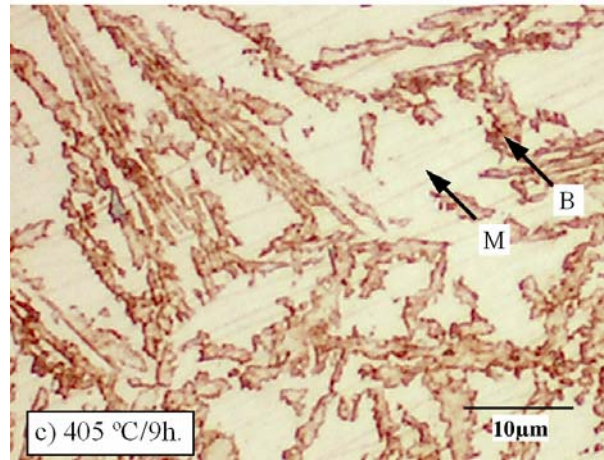
Figure 7 –The temporal evolution of the volume fraction of the BCC phase (a) and variation in the edge width parameter of the FCC phase as a function of the volume fraction of the BCC phase (b).



a)



b)



c)

Figure 8 Optical micrographs illustrating the microstructures of the steel after isothermal transformation, a) for 9 hours at 283 °C, b) 8 hours at 335 °C and c) 6 hours at 405 °C. The arrows inserted in the figures show bainite packets (B), retained austenite (RA) and martensite (M).

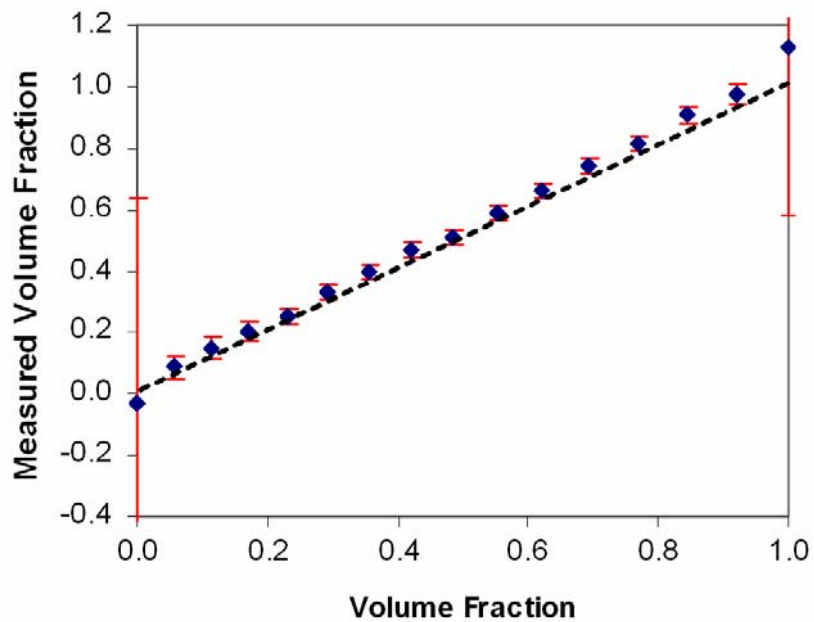
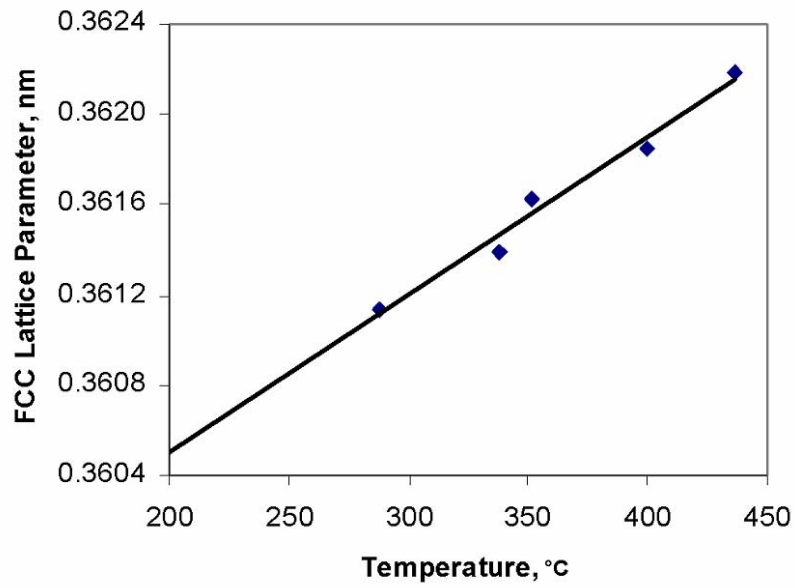
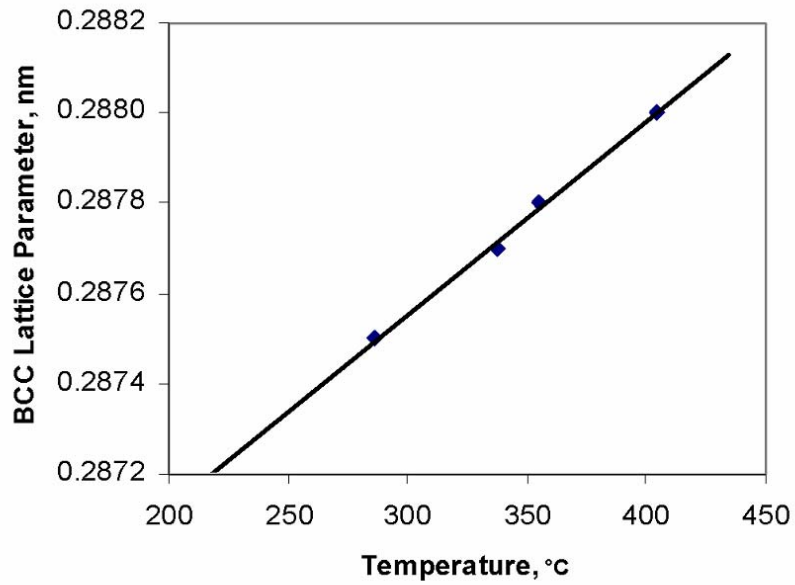


Figure 9 – Measured volume fraction of the BCC phase derived from BET experiments vs. the true volume fraction of the BCC phase for samples with various combinations of disks comprised of interstitial free (BCC) and 304 stainless (FCC) steels.



(a)



(b)

Figure 10 Lattice parameters derived from BET measurements as a function of temperature for (a) the FCC phase (b) the BCC phase. Note: errors in measurements are within the symbol size.

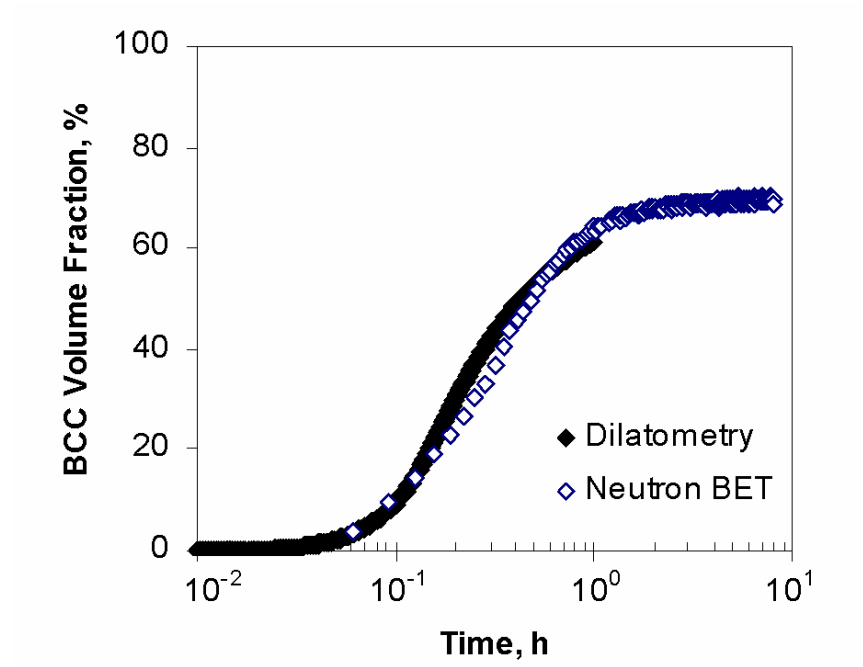


Figure 11 Comparison of the bainite formation kinetics at 335 °C measured by neutron BET and dilatometry.

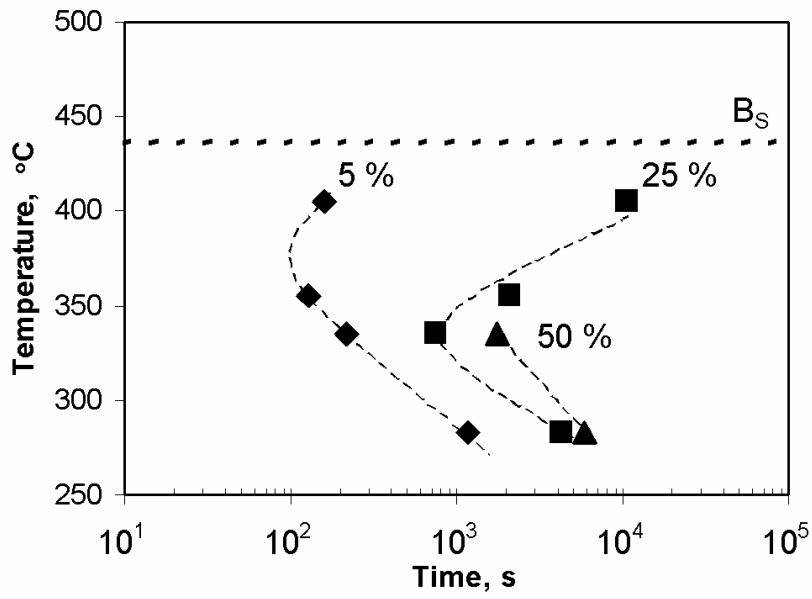


Figure 12 TTT diagram for the decomposition of austenite. The dashed line represents the bainite start temperature calculated by Steven and Hayes [45]

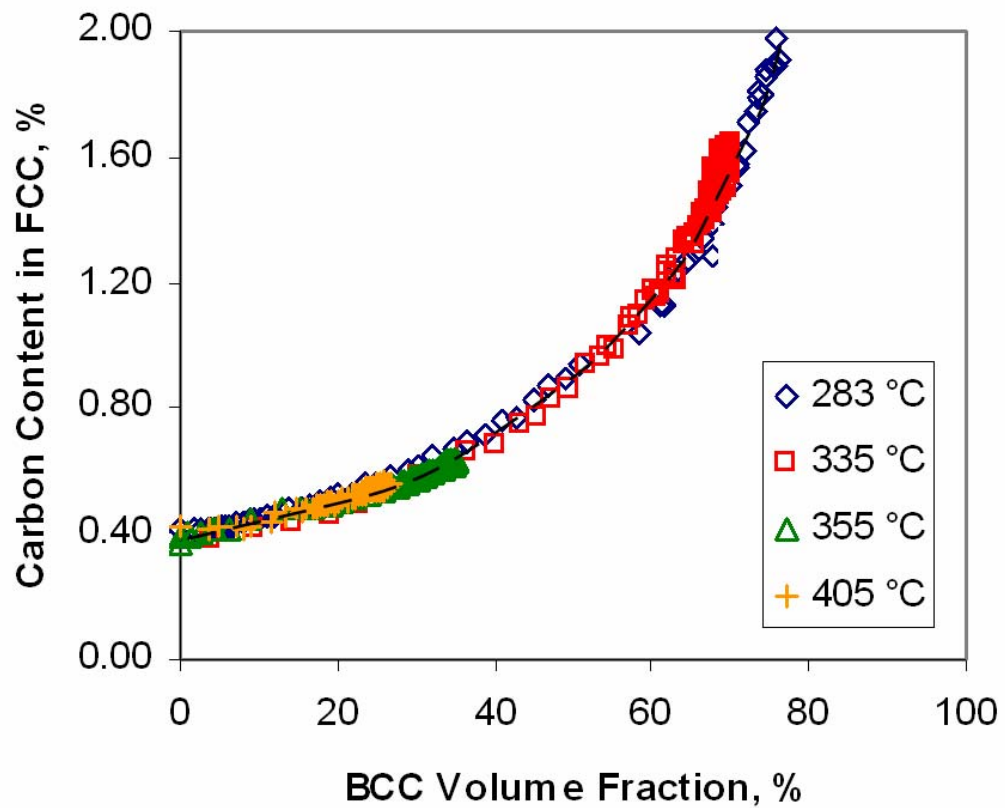


Figure 13 Changes of carbon concentration (wt%) as a function of the BCC volume fraction transformed. The experiments were conducted at 283 °C, 335 °C, 355 °C and 405 °C. The dashed line represents the carbon concentration calculated by using the mass balance.